JMATPRO

Journal of Advanced Materials and Processing
9 (4): 23-34, Autumn 2021
http://jmatpro.iaun.ac.ir
20.1001.1.2322388.2021.9.4.3.5

Research Paper

The Effect of Morphology of SOFC Layers Made by 3D Printer on the Electrochemical Properties of the Cell

Keyvan Mirzaee Fashalameh[1,2*], Zahra Sadeghian[3], Ramin Ebrahimi[1]
1. Department of Materials Science and Engineering, Shiraz University, Shiraz, Iran
2. Department of Engineering, payam Noor University (PNU), Tehran, Iran
3. Research Institute of Petroleum Industry (RIPI), Tehran, Iran

ARTICLE INFO

Article history:

Received 18 July 2021
Accepted 2 October 2021
Available online 1 November 2021

Keywords:
Solid oxide fuel cell
3D printing
Electrochemical properties
Electrical conductivity

ABSTRACT

The microstructure and properties of solid oxide fuel cell (SOFC) connected to the fabrication process are discussed in this paper. In this research, we investigate the relationship between electrochemical performance in solid oxide fuel cells and the evolution of the morphology of its electrodes. This work fabricated a planar multilayer anode-supported, anode functional layer (AFL), electrolyte, and cathode solid oxide fuel cell through slurry-based 3D printing. After drying and sintering, scanning electron microscope (SEM) images a multilayer porous structure with large pores up to several microns and smaller pores of 100 nm, and the constituent particles' microstructure for anode-cathode layers were observed. The electrolyte layer structure was dense and without pores. In the study of electrochemical properties, the maximum power density at the output voltage of 0.5 V was achieved at 0.84 W/cm^2 at an open-circuit voltage (OCV) of 1.06 V at 800 °C with H_2 gas as fuel. The impedance curve values under open-circuit voltage were 0.23 V and 1.25 V at high and low frequencies, respectively.

Citation: Mirzaee Fashalameh, K., Sadeghian, Z., Ebrahimi, R. (2021) The Effect of Morphology of SOFC Layers Made by 3D Printer on the Electrochemical Properties of the Cell, Journal of Advanced Materials and Processing, 9 (4), 23-34. Dor: 20.1001.1.2322388.2021.9.4.2.4

---

[*] Corresponding Author.
E-mail address: keyvan_feshalame@yahoo.com

1. Introduction

Fuel cells are some sort of energy converter that convert chemical energy directly into electrical energy. Fuel cells function the same as batteries; however, in contrast to batteries, they will never stop working as long as they are supplied with fuel and do not need recharging [1]. Various types of fuel cells, have been produced to date, but since the chemical reaction results in a high temperature, the solid oxide type of these cells known as solid oxide fuel cells (SOFCs), is more attractive. The performance of a SOFC is based on the following electrochemical reaction [2]:

$2H_2(g) \Rightarrow 4H^+ + 4e^-$ (anode reaction)
$O_2(g) + 4H^+ + 4e^- \Rightarrow 2H_2O(l)$ (cathode reaction)
$2H_2(g) + O_2(g) \Rightarrow 2H_2O(l)$ (cell reaction)

SOFCs have so far been produced using various methods, including screen printing [3], sol-gel [4, 5], electroless plating [3], electrophoretic deposition [3], electrochemical vapor deposition (EVD), physical vapor deposition (PVD) [6, 3], and thermal spray (atmospheric plasma spray; APS) [7]. In recent years, the use of the 3D printing method for producing fuel cells has received attention from a few scientists [8, 9].

A desirable generation of energy in a SOFC necessitates sufficient thickness and appropriate morphology for each of the layers, including the anode support layer, the AFL, the electrolyte layer, and the cathode layer. In this regard, the size and distribution of the particles forming the base anode and the functional anode must be in such a way as to yield a porosity of 20-30%. As the porosity exceeds 30%, the electrical conductance decreases gradually [10-14]. The electrolyte layer must be condensed and nonporous; thus, particles of this layer are very fine and uniformly distributed [15-17]. The cathode layer is deposited on the electrolyte layer and requires a porosity of nearly 40%. The particle size and distribution of the cathode layer affect its degree of porosity [18-21]. Excessive porosity in the anode and cathode layers would reduce their interface with the electrolyte layer, reducing the cell's effective reaction surface, thereby reducing the region of triple-phase boundaries (TPBs) and, consequently, the electrochemical properties and the fuel cell efficiency. The TPBs are the area of connection between the three phases of electrolyte, electrode, and fuel gases, and all reactions occur within these three phases [22]. Low porosity in the electrodes causes disturbance in the fuel gas and the oxygen gas flow, resulting in improper reaction [23]. Therefore, as both high porosity and low porosity result in disturbance, an appropriate degree of porosity is of interest.

Suitable thickness in a fuel cell is one factor that improves its electrochemical performance. The performance temperature of the cell for an electrolyte layer with a thickness of 200 µm is within the range of 600-1000 ˚C [1]. A reduction in the thickness of the electrolyte to 10-12 µm reduces its electrical resistance such that the same amount of energy can be generated at a temperature of 150-200 ˚C [24]. For the anode layer, the maximum efficiency and the maximum power density are obtained when the anode layer has a medium thickness of about 0.5 mm. Thinner anodes can utilize less amount of the produced H_2, which in turn leads to a lower average current density, efficiency, and power density. However, higher amounts of H_2 are produced in thick anode layers, which increases the exothermic reaction rate, leading to a decrease in cell performance [25].

In the present research, the deposition of the anode, electrolyte, and cathode layers was initially performed by a 3D printer. Subsequently, sintering the layers was followed by examining the structure, porosity, density, and thickness of the layers by XRD, SEM, and mapping. The other stages of the present work include determining the electrochemical properties such as polarization, current density, power density, generated voltage by the I-V diagram, and the impedance of the fabricated cell.

2. Experimental Procedure

2.1. The cell layers fabrication

To fabricate the cell layers, the percentage composition of materials according to Table 1 was used. The 8 mol% Y_2O_3-stabilized ZrO_2 (8 yttria-stabilized zirconia; 8YSZ) was applied with an average particle size of about 0.25 µm (Tosoh Corporation, Japan). The NiO powder was used with an average particle size of about 0.25 µm (Merk, Germany). The powders have been mixed with a composition of 65 wt% NiO-YSZ (60:40 wt%)-35 wt% and with the pellet maker, parts with an approximate thickness of 0.5 to 2 mm and a diameter of 20 mm as a support layer were made. The pellet at a thermal rate of 3 ºC/min was heated to 180 °C for one hour and dried. Then by 3D printer, an AFL layer with a combination of NiO-YSZ and ethanol solvent, additives such as dibutyl phthalate (DBP), polyvinyl chloride (PVC), and polyethylene glycol (PEG) at a rate of 700 mm/min on pellet about 40 microns thick was printed. The AFL layer was also dried with the above conditions. The obtained substrate was heated to 600 °C with 2 h soaking time to ensure removal of pore former, and then it was sintered at 1200 °C for 4 h. Finally, the pellet was heated to 1000 °C for 4 h in a tube furnace with a hydrogen atmosphere to reduce the nickel oxide to nickel element. After the first layer, the YSZ electrolyte slurry was directly spread at a speed of 2000 mm/min and a thickness of about 20 microns on the green AFL layer by the 3D printing process. The sample was allowed to dry at 90 °C and then co-sintered at 1400 °C for 4 h with a heating rate of 1 °C $\min^{-1}$ before 600 °C and 2 °C $\min^{-1}$ after 600 °C in an air atmosphere to remove the organics to prevent crack (formation half-cell formation). To cool, it was first cooled from 1400 to 600 °C at a thermal rate of -3 ºC/min for 3.5 h and then removed from the oven and cooled in the open air to room temperature. After that, for the fabrication of a complete solid oxide cell, lanthanum strontium manganite (LSM) solid powder with solvent materials and additives was produced as a slurry suitable for the nozzle and finally, the cathode layer was deposited by a 3D printer on the electrolyte layer set with a speed of 700 mm/min and a thickness of 40 microns. The printed structures were dried at 90 °C, then heated at 600 °C with 1 h holding time, and finally sintered at 1200 °C for 2 h with a rate of 5 °C/min in air. Fig. 1 shows the 3D printer during printing, layer formation, and SEM image of the cross-section and surfaces of the anode, cathode and electrolyte layers.

Table 1 The composition of slurry for deposition of different layers

Composition(%) layer type	YSZ	NiO	LSM	PEG	PVC	DBP	Ethanol-Tolouen (1:1) solvent
AFL layer	2.8	2.8	-	0.1	0.1	0.1	94.1
Electrolyte layer	10.7	-	-	0.1	0.1	0.1	89
Cathode layer	-	-	1.45	0.1	0.1	0.1	96.8

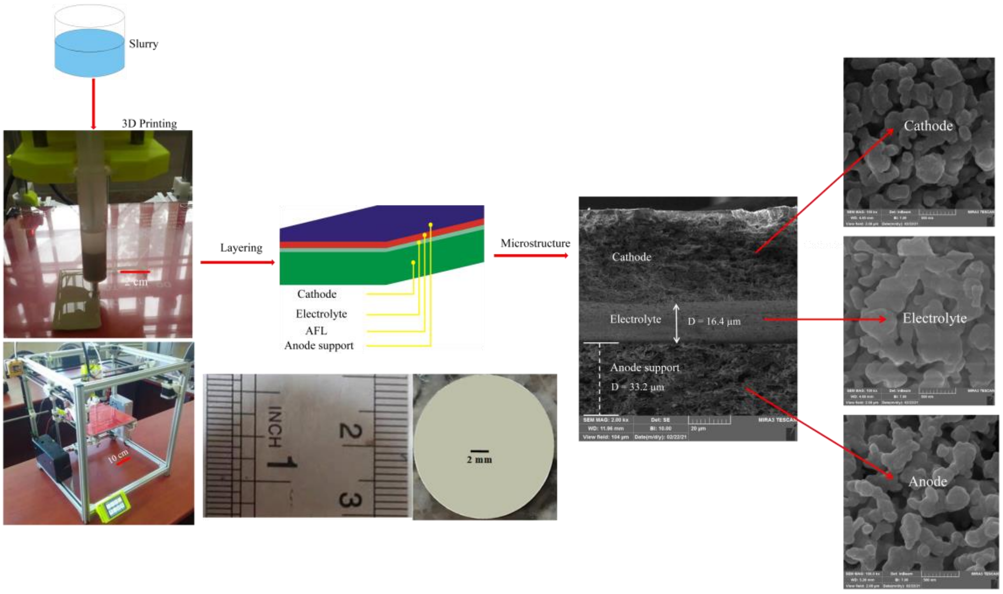

Fig. 1. The picture of the 3D printer during printing, layer formation and SEM image of the cross-section and surfaces of the anode, cathode and electrolyte layers

2.2. Characterization

The open porosity of the anode pellets was calculated by Archimedes' water displacement method (ASTM C373-2014). To detect phases existing elements, determine the microstructure and thickness of anode, cathode, and electrolyte layers and connections between layers [26] of X-ray diffraction (XRD) tests by the device (Equinox 3000, Intel: using Cu-Kα (λ = 0.154 nm), Scanning electron microscopy (SEM), energy dispersive X-Ray analysis (EDX) and mapping tests were performed using the device Field emission *scanning electron microscopy* (FE-SEM; Mira 3 XMU, Tescan). To obtain the electrochemical properties, the current density-voltage-power (I-V-P) curve was first measured by (Linear sweep voltammetry) with a scanning rate of 5 mV/s [27] and a constant flow and purity of oxygen at variable temperatures of 700, 750, and 800 ºC. Impedance spectra were measured in combination with the electrochemical interface in a frequency range of 0.1 Hz to 910 kHz with a voltage range of 10 mV under open-circuit voltage (OCV) using an impedance device (Solartron Instruments, Hampshire, UK).

3. Results and discussion

3.1. Morphology and microstructure of the cell

Fig. 2 shows the XRD patterns of the anode support, AFL, cathode and electrolyte components and the reference phases Miller indices. the presence of NiO phase observed the peak splitting of the cubic phase in adapting with the standard XRD data of ICDD#00-047-1049, at $2\theta = 37.060^0, 43.095^0$ and 62.620^0 which are indicated (111) (200) and (220) plans, respectively [28-30]. Also, the presence of the Ni phase exhibited the only single peaks that assigned to (200) and (220) at 51.86^0 and 76.39^0 of 2θ, respectively [29]. As the presence of YSZ phase of the cubic phase in adapting with the standard XRD data of ICDD#00-048-0224, the peaks at 30.1°, 34.9°, 50.2°, and 59.6° of 2θ, corresponding to the (111), (200), (220) and (311) planes, respectively [29- 30]. The other peaks observed at an angle (2θ) of 32.40° and 32.70° which have been identified as LSM with the standard XRD data of ICDD#00-040-1100 [31] corresponds to (110), (200), crystal planes, respectively.

The EDX and mapping images (Fig. 3a,b) obtained from the anode layer indicate the presence of the O, Ni, Zr, and Y elements in the anode layer before the reduction, in which all the elements, except O, are shown after reduction. Carbon was added to the anode before the reduction to create suitable porosity, as shown in Fig. 3b (right).

As can be seen in Fig. 3c (left), the NiO-YSZ layer had a dense structure with stochastic and heterogeneous porosity before the reduction. As the anode is placed in the reductive atmosphere (5%H_2-95%Ar), NiO is gradually reduced to Ni. According to Fig. 3c (right), the reduction is followed by the formation of the porous anodes of Ni-YSZ. The presence of carbon during the reduction operation results in the production of CO and CO_2 gases, the consequence of which is a higher porosity [13]. Based on the SEM image in Fig. 3c (right) and the Archimedes test, a porosity of 28% was estimated for the anode. The effective factors in the degree and formation manner of porosity and the microstructure of the anode layer include the size, amount, and distribution of the NiO and YSZ particles and the amount of carbon [13]. Heterogeneous distribution and inappropriate amount and size of the anode particles prevent a suitable connection between the anode layer and the electrolyte, which causes a reduction in the TPBs region, leading to decreased electrochemical properties. The average particle size of the porosity (Fig. 3c (right)) is nearly 5.0 μm, which is consistent with previous work [23]. The existence of appropriate porosity along with a uniform microstructure throughout the layers can improve the electrochemical properties of the cell. However, high porosity, large size, and non-homogeneous distribution reduce the contact surface between the electrode and electrolyte layers and the surface area of the TPBs region, resulting in the declined electrochemical properties. Moreover, low porosity prevents the appropriate passage of the electron flow and appropriate electrochemical reaction. Therefore, a 30% porosity with uniform distribution is helpful for appropriate electrochemical properties. Similar results were reported previously [14,15,18,23,33-35]. According to these results, it can be concluded that the 3D printer has good capability for ceramic slurry printing to create appropriate anode layers.

The mapping images in Fig. 4a and EDX image in Fig. 4b, obtained from the electrolyte layer, prove the presence of Zr and Y elements in the electrolyte layer. The SEM images of the electrolyte membrane (Fig. 4c) indicate a condensed and uniform electrolyte layer as well as a very limited, dispersed, and, of course, superficial porosity. The electrolyte density was tested by the nitrogen passage test, in which the nitrogen gas passage through the electrolyte was very insignificant and approximately equal to zero, indicating the very insignificant porosity of the electrolyte layer. Some of the small pores in the electrolyte were eliminated due to the sintering temperature (about 1400 ˚C) of the electrolyte layer, resulting in a dense layer with very limited and fine porosities. Factors affecting the density of the electrolyte layer generally include the particle size and uniformity as well as the quality and amount of sintering in terms of time and temperature. Similar results were reported previously [14,15,18,32-35].

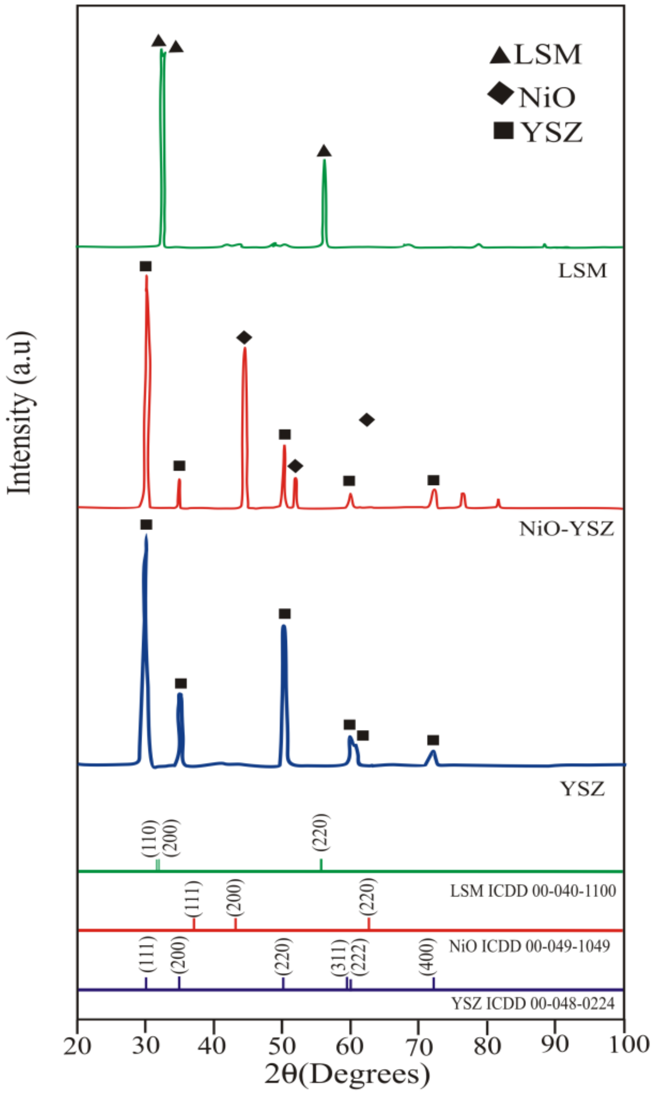

Fig. 2. XRD patterns of NiO-YSZ, YSZ and LSM synthesized layers

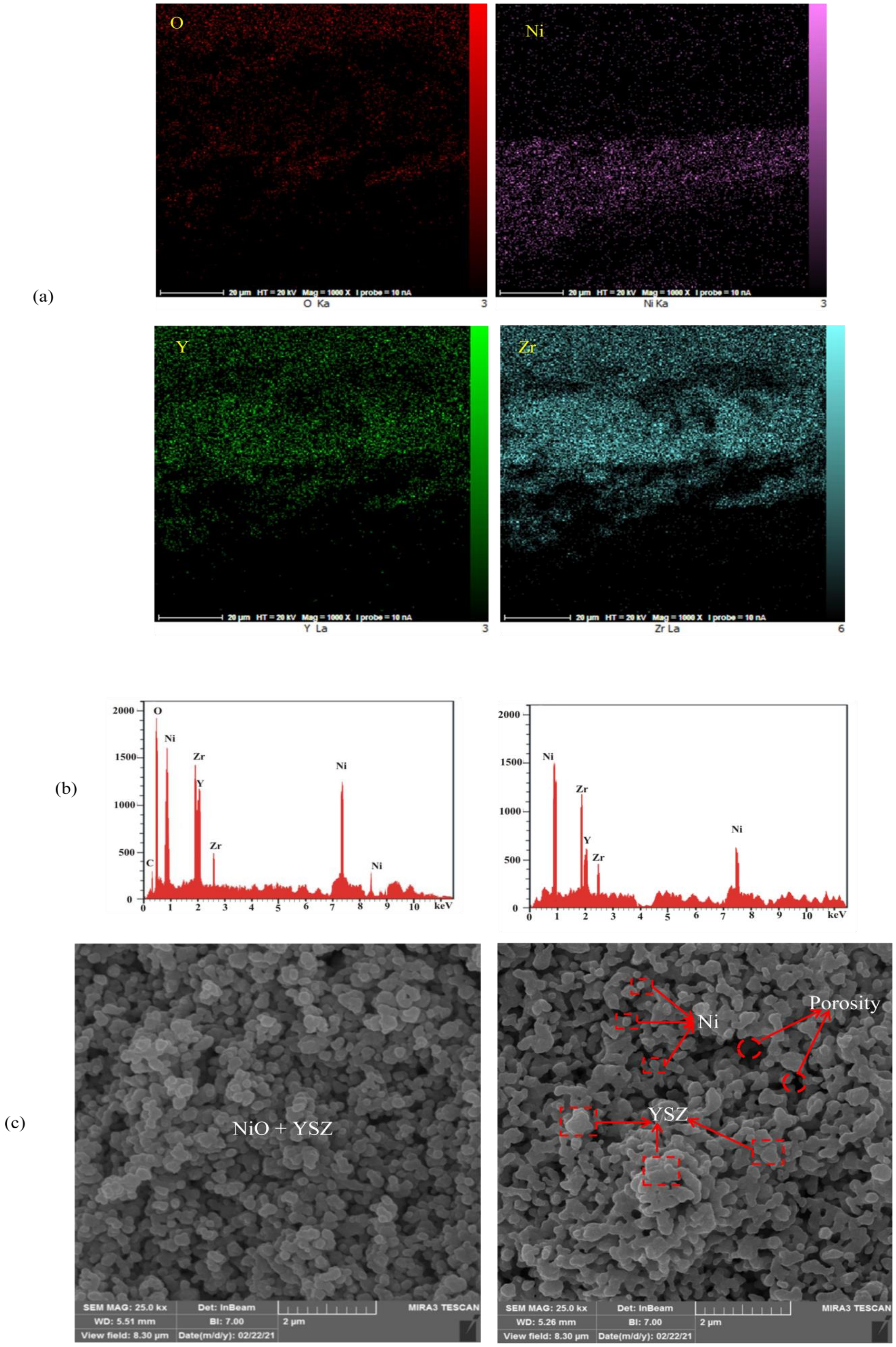

Fig. 3. (a) The elemental mapping images, (b) EDS spectrums of anode support, before reduction (left) and after reduction (right) and (c) (left) FE-SEM images anode pellet before reduction and (right) FE-SEM images anode pellet after reduction by H_2

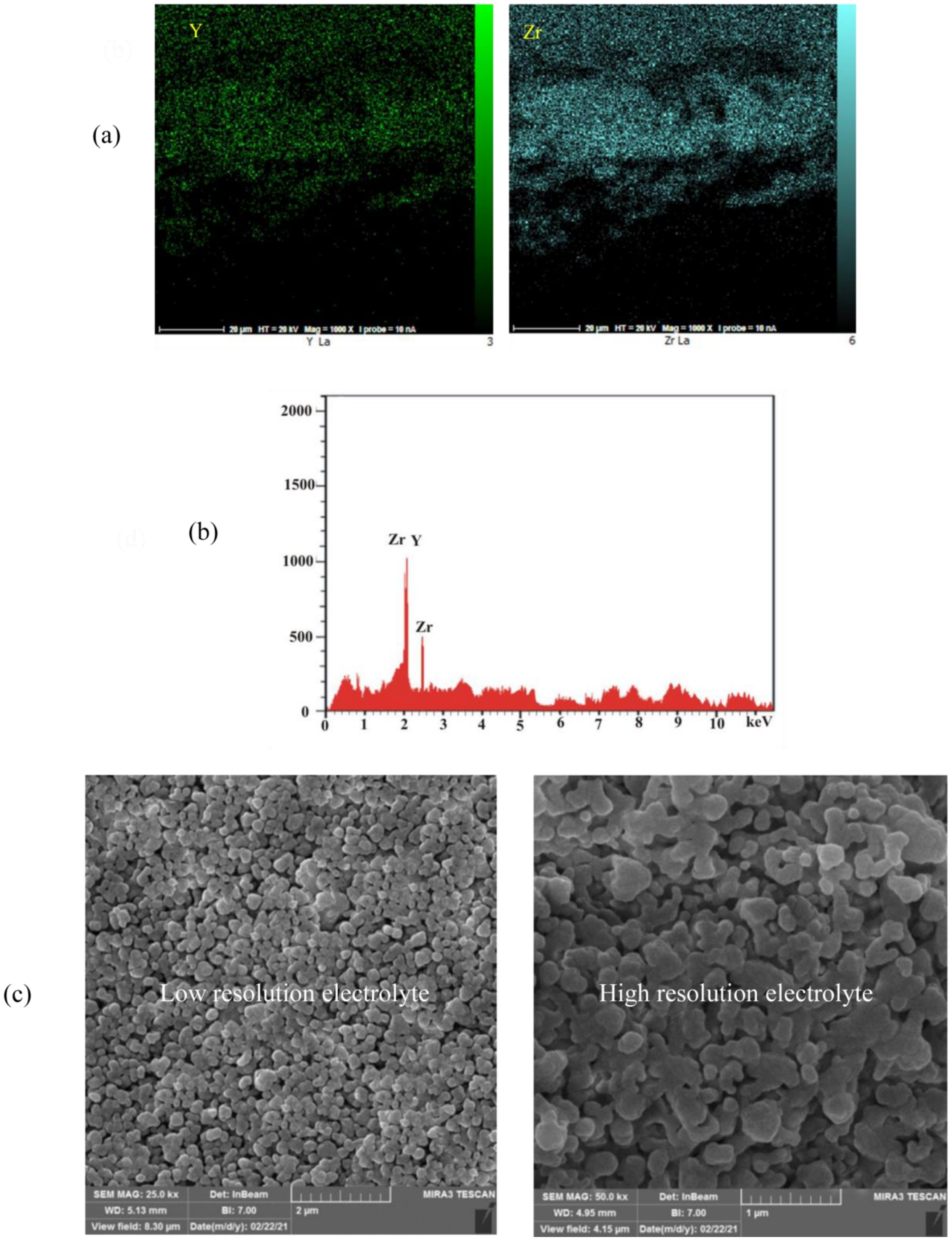

Fig. 4. (a) elemental mapping images of electrolyte layer, (b) EDS spectrums of electrolyte layer, and (c) (left) low-resolution electrolyte layer FE-SEM image, and (right) high-resolution electrolyte layer FE-SEM image

In SOFCs, LSM as a conductor at high temperatures is commonly used for the cathode. The elemental analysis of mapping and EDS spectrum (Fig. 5a,b) obtained from the cathode layer proves the Sr, La, and Mn presence in this layer. Regarding the microstructure, the SEM images of the cathode layer (Fig. 5c) illustrate the fine size and uniform distribution of the LSM particles. The electrolyte ions are reduced in the cathode. Therefore, the first feature of the cathode is that it must be able to quickly transfer the oxygen to the TPBs through its porous surface.

Also, the cathode must have a good degree of porosity in order to be able to transfer oxygen ions well after reduction. Since the oxygen molecule and ion are larger than hydrogen, the cathode must necessarily have a higher porosity than the anode to facilitate the passage. The SEM images of the cathode layer (Fig. 5c) indicate the presence of a relatively porous layer. The cathode porosity was estimated to be 40% using the SEM images and the

Archimedes standard method. As reported previously [36], the porosity range of 40-50% provides the best conditions for the suitable gas passage of LSM. The following Archimedes formula was used to measure the porosity of the cathode layer [36]:

$$p_0 = \frac{W_b - W_a}{W_b - W_c}$$

where W_a, W_b, and W_c indicate the weight of the dry layer, the weight of the water-saturated layer, and the weight of the layer immersed in distilled water (with a density of 1g/cm^3), respectively [36]. Similar results were obtained in previous studies [19, 21]. Modifying the microstructure of the cathode significantly affects the resistance of the whole cell. A reduction in the grain size, provided that the high porosity is maintained, is very effective for improving the current density [25]. Fine-grained particles increase the density of the TPBs region and, thus, cause the rapid penetration of gas and reduction of resistance against polarization, leading eventually to increased electrochemical performance of the cell [37, 38].

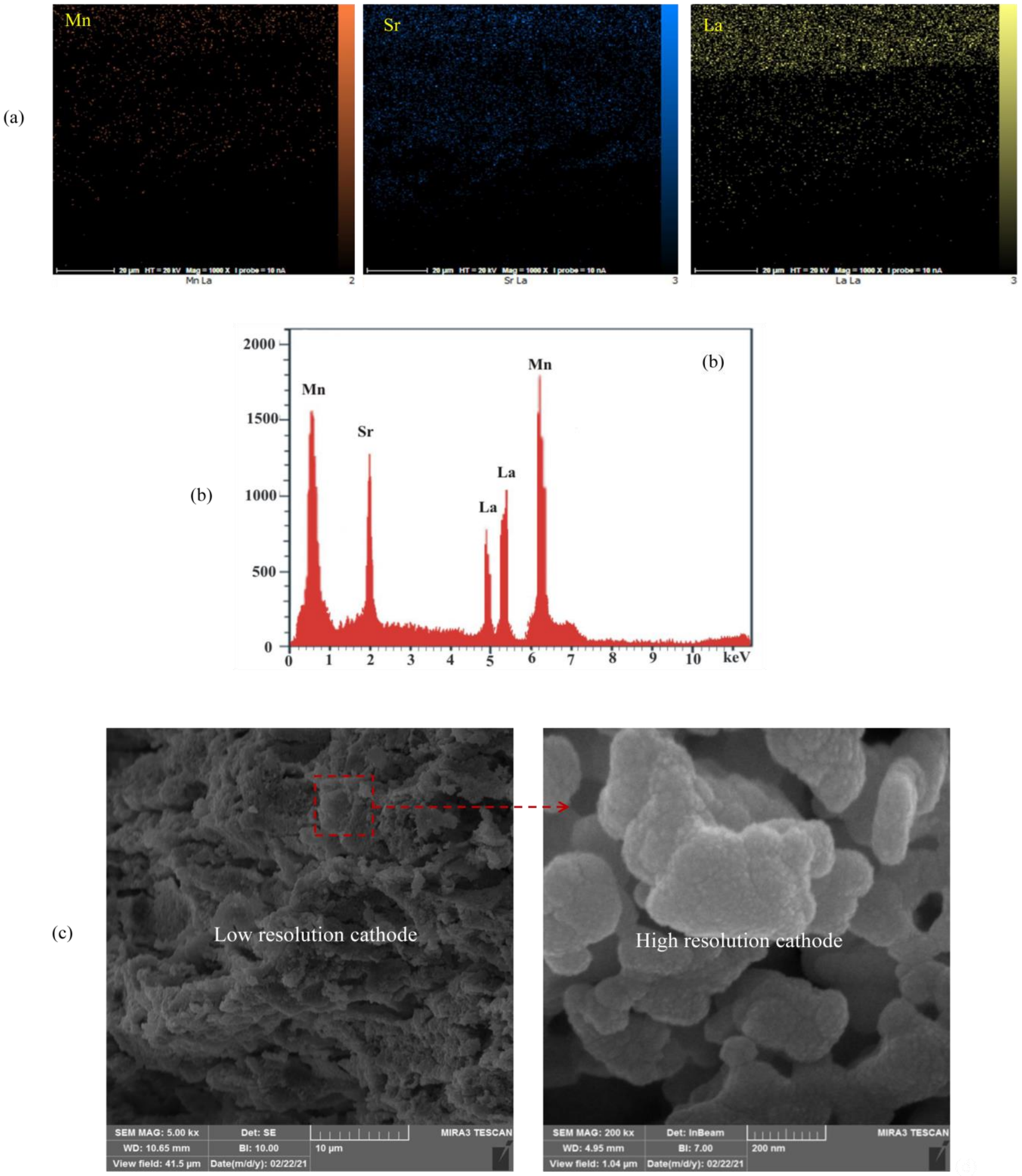

Fig. 5. (a, b) The elemental mapping images and EDS spectrums of cathode layer, respectively, and (c) FE-SEM images of the cathode layer.

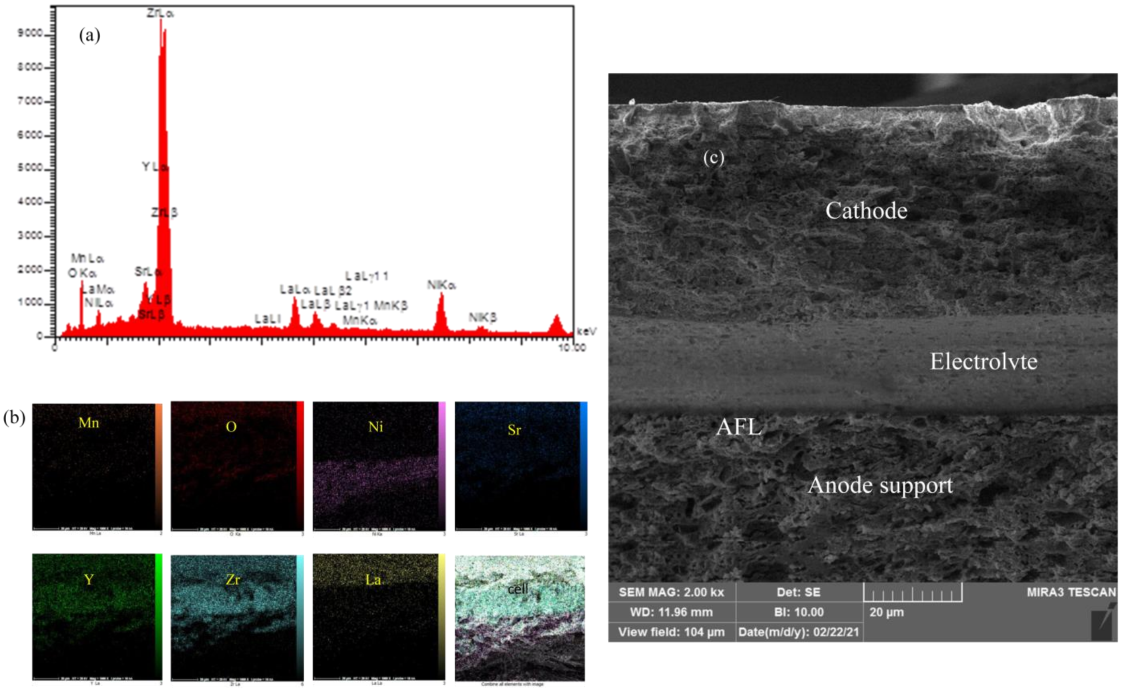

Fig. 6. (a, b) EDS spectrums and elemental mapping images of cell layers, and (c) Cross-section FE-SEM images of cell layers

3.2. Electrochemical performance of cells

3.2.1. Current density-voltage-power (I–V–P) curves

According to Fig. 7, it is observed that the open-circuit voltage (OCV) at the lowest current density is about 1.06 volts, which is in good agreement with the values estimated by Nernst's law. The exhibited lower OCVs than the Nernst theoretical voltage (1.11V) can be related to the relatively dense microstructure of the electrolyte [39,40]. This curve shows that as the temperature increases, the current density and power density increase, so the voltage decreases. Therefore, at maximum temperature, the maximum power densities at the output voltage of 0.5 V and current density 1.43 A.cm^2 were reached 0.57, 0.68, and 0.84 W/cm^{-2} at 700, 750, and 850 ˚C, respectively. The obtained maximum power density at 800 °C is about up to 1.8 times is higher than the reported values for anode supported SOFC with similar compositions [41,42]. The high value of power density in the present work can be related to the composition and microstructure of electrodes and electrolytes. As mentioned, the high porosity microstructure of anode substrate by using pore former has an important role in the enhancement of performance of the cell. Also, a fine uniform structure across the layers can improve power density. These results are consistent with the report presented in reference [43] that a 3D printer makes solid oxide fuel cell layers.

3.2.2. Impedance measurement

One of the preferred methods of impedance displays is the Nyquist curve. In this display format, the data are plotted in complex coordinates including the real impedance Z' and the imaginary impedance Z" in the range of the excitation frequency. To determine the impedance, a small alternating current (AC) of 5-10 mV is applied at a certain frequency. This wave with a certain frequency after contacting the surface of the cell causes turbulence in the arrangement of atoms and, therefore, the number of frequency changes. The magnitude of this turbulence is actually the amount of resistance to current flow. These changes are measured by a frequency analyzer (FRA). In this analyzer, there are electrical circuits that calculate the changes made in these circuits by complex numbers. Therefore, the impedance Z (ω) is calculated as a complex number and has two parts, real and imaginary. The real part of it is due to the presence of resistors in the circuit and is known as (Z'), which is expressed by the Z_R=R equation. The imaginary part is related to other components of the circuit such as magnetic field radiation, capacitor and inductor and the like, which is expressed by (Z″), which with its equation is as follows:

$$Z_C = \frac{1}{J\omega C} \quad (1)$$

Fatemeh Sadeghzadeh et al. [37] reported that if the frequency is at its highest, Zc will be to zero in measuring impedance. In this case, the impedance will be related only to the real component, which is significantly related to the resistance between the contact layers and the intentional conductivity of the electrolyte and if the frequency is at its lowest value and towards zero, the value of Zc reaches its highest value and the total impedance is related to the imaginary part. Also, the contact resistance between electrodes' surfaces and the current collector can affect total resistance. As well ohmic resistance of cathode has a remarkable role in total resistance. Therefore, the modification of cathode microstructure remarkably affects total resistance. These values correspond to previously obtained information from sources [44-46].

Cell conduction behaviour is investigated by impedance spectroscopy under open-circuit conditions at 800 °C. According to Fig. 8, the impedance value at Zc=0 and the first intersection with the real ohmic axis R are equal to 0.23 Ωcm^{-2}, in which case R is the resistance between the layers related to the electrolyte layer thickness and the connection between the YSZ electrolyte and the Ni-YSZ electrode. The second intersection with the real axis and the tracking of the first and second intersection exhibit the total resistance and the electrode polarization resistance, respectively at low frequencies [44,47]. In this case, according to Fig. 8, the total resistance at high values of Zc will be 1.25 Ωcm^{-2}.

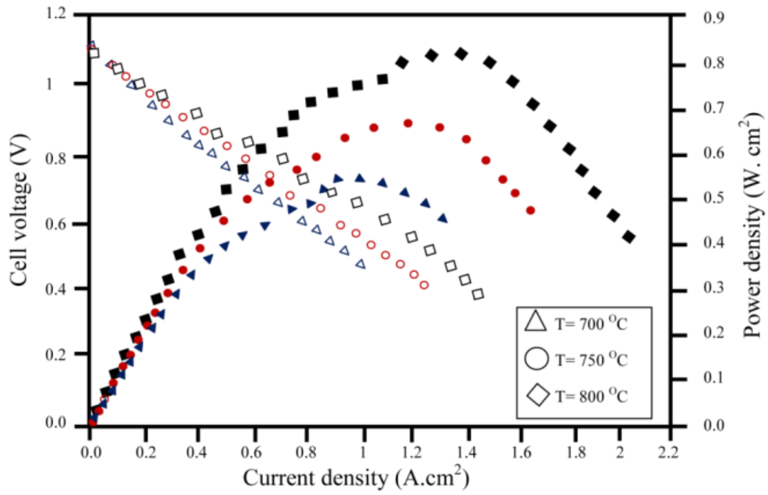

Fig. 7. I-V-P curves of the slurry-based 3D-printed cell at 700, 750, and 800 °C in H_2 fuel with a flow rate of 50 mL min^{-1}

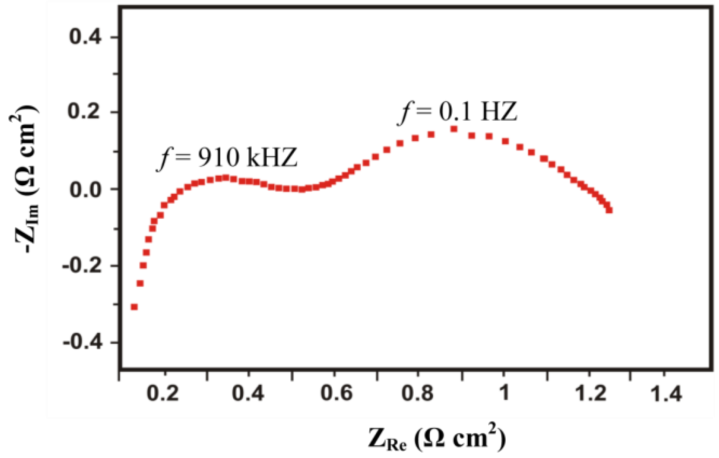

Fig. 8. Impedance spectra of the cell at 800 °C under OCV condition using H_2 fuel.

4. Conclusion

In this research, the production of solid oxide fuel cells with Ni-YSZ/Ni-YSZ (AFL)/YSZ/LSM layers was done using a new method using a 3D printer and new solvents additives. The Ni-YSZ (50:50 wt%), YSZ, and LSM layers were successfully fabricated on Ni-YSZ (60:40 wt%) support by slurry-based 3D printing. The particle distribution of the AFL and cathode layers with a thickness of about 40 µm is uniform, and the distribution of its pores is large, medium, and small cavities. The electrolyte layer is completely dense and about 20 µm thick. Solid load content can control the microstructure and porosity in slurry, deposition rates, and sintering conditions. In this case, a single cell produced by a 3D printer was able to produce a maximum power density of 0.84 W/cm^2 at 800 °C. This porous structure of the anode and cathode and the dense structure of the electrolyte increases the active region and increase the penetration and effect of the gas, which in turn leads to an increase in the electrochemical performance of the cell.

References

[1] H. Buchkremer, U. Diekmann, D. Stöver, “Component Manufacturing and Stack Integration of Anode-supported Planar Sofc System”. Proceedings of the Second European Solid Oxide Fuel Cell Forum, Vol. 1, 1996, pp. 221-228.

[2] H. O, K. Nozawa, “Development of Highly Efficient Planar Solid Oxide Fuel Cells”, Special Feature, vol. 6, 2008, pp. 680-690

[3] J. H. Song, S.-I. Park, J.-H. Lee, H.-S. Kim, “Fabrication characteristics of an anode-supported thin-film electrolyte fabricated by the tape casting method for IT-SOFC”, Journal of materials processing technology, vol. 198, 2008, pp. 414-418,

[4] Kim. S. D, Lee. J. J. Moon, H. Hyun, S. H. Moon, J. Kim. J, “Effects of Anode and Electrolyte Microstructures on Performance of Solid Oxide Fuel Cells”, Journal of Power Sources, vol. 169, 2007, pp. 265-270.

[5] Pierre, A. C, Introduction to Sol-gel Processing, Springer, New York, 1998.

[6] R. Mücke, “Introduction to SOFC Technologies Manufacturing of SOFCs”, Joint European Summer School for Fuel Cell and Hydrogen Technology Viterbo, Italy, 2011,198.

[7] S. Y. Park, C. W. Na, J. H. Ahn, R. H. Song, J. H. Lee, “Preparation of highly porous NiO–gadolinium-doped ceria nano-composite powders by one-pot glycine nitrate process for anode-supported tubular solid oxide fuel cells”, Journal of the Asian Ceramic Societies, vol. 2, 2014, pp. 339-346.

[8] J. C. Ruiz-Morales, A. Taranco´n, J. Canales-Va´zquez, J. Me´ndez-Ramos, L. Herna´ndez-Afonso, P. Acosta-Mora, J. R. Marı ´n Ruedac and R. Ferna´ndez-Gonza´leza, “Three dimensional printing of components and functional devices for energy and environmental applications”, Energy & Environmental Science, Vol. 10, 2017, pp. 846-860

[9] M. M. Torrell, P. Leone, A. Tarancón, “Three-dimensional printed yttria-stabilized zirconia self-supported electrolytes for solid oxide fuel cell applications” Journal of the European Ceramic Society, Vol. 39, 2019, pp. 9-16.

[10] H. Itoh, T. Yamamoto, M. Mori, T. Horita, N. Sakai, H. Yokokawa, et al, “Configurational and electrical behavior of Ni-YSZ cermet with novel microstructure for solid oxide fuel cell anodes”, Journal of the Electrochemical Society, vol. 144, 1997, pp. 641-646.

[11] S. Pratihar, R. N. Basu, S. Mazumder, H. S. Maiti, “Electrical conductivity and microstructure of Ni-YSZ anode prepared by liquid dispersion method”, Electrochemical Society Proceedings, Vol. 1999-19, 1999, pp. 513-521.

[12] J. H. Lee, H. Moon, H. W. Lee, J. Kim, J. D. Kim, K. H. Yoon, “Quantitative analysis of microstructure and its related electrical property of SOFC anode, Ni–YSZ cermet”, Solid State Ionics, vol. 148, 2002, pp. 15-26.

[13] D. Medvedev, J. Lyagaeva, G. Vdovin, S. Beresnev, A. Demin and P. Tsiakaras, “A tape calendering method as an effective way for the preparation of proton ceramic fuel cells with enhanced performance”, Electrochimica Acta, vol. 210, 2016, pp. 681-688.

[14] Dehua, D. Jianfeng, G. Xingqin, L. Guangyao, Meng, “Fabrication of tubular NiO/YSZ anode-support of solid oxide fuel cell by gelcasting”, Journal of Power Sources, Vol. 165, 2007, pp. 217–223.

[15] D. Dong, Y. Huang, X. Zhang, L. He, C. Z. Li, H. W, “Shape forming of ccs with controllable microstructure by drying-free colloidal casting”, Journal of Materials Chemistry, Vol. 19, 2009, 7070–7074.

[16] G. B. Balazs, R. S. Glass, “AC impedance studies of rare earth oxide doped ceria”, Solid State Ionics, vol. 76, 1995, pp. 155-162.

[17] Y. Arachi, H. Sakai, O. Yamamoto, Y. Takeda and N. Imanishai, “Electrical conductivity of the ZrO_2–Ln_2O_3 (Ln= lanthanides) system”, Solid State Ionics, vol. 121, 1999, pp. 133-139.

[18] J. P. Viricelle, C. Pijolat, B. Riviere, D. Rotureau, D. Briand, N.F. de Rooij, “Compatibility of screen-printing technology with micro-hotplate for gas sensor and solid oxide micro fuel cell development” Sensors and Actuators. Vol. B 118, 2006, pp. 263–268.

[19] G.N. Almutairi, Y. M. Alyousef, F.S.Alenazey, S. A Alnassar, H. Alsmail, M. Ghouse, “Electrochemical Characteristics of $La_{0.65}Sr_{0.3}MnO_3$ and $La_{0.8}Sr_{0.2}MnO_3$ Nanoceramic Cathode Powders for Intermediate Temperature Solid Oxide Fuel Cell (SOFC) Application”, Int. J. Electrochem. Sci. Vol. 12, 2017, pp. 8148 – 8166.

[20] G. Almutairi1, F. Alenazey,Y. Yousef1, B. Alshammari2, “Alanine Assisted Synthesis and Characterization of $La_{0.65}Sr_{0.3}MnO_3$ (LSM)”, Int. J. Electrochem. Sci. Vol. 12, 2017, pp. 11616 – 11632.

[21] C. Levy, Yu. Zhong, C. Morel, S, Marlina, A. Assisted. “Thermodynamic Stabilities of $La_2Zr_2O_7$ and $SrZrO_3$ in SOFC and Their Relationship with LSM”, Synthesis Journal of The Electrochemical Society. Vol. 157, 2010, B1597-B1601.

[22] J. Fergus, R. Hui, X. Li, D. P. Wilkinson, J. Zhang, Solid oxide fuel cells: materials properties and performance, CRC press, 2016. Pp. 156.

[23] S. Pratihar, R. N. Basu, S. Mazumder, H. S. Maiti, “Electrical conductivity and microstructure of Ni-YSZ anode prepared by liquid dispersion method”, Electrochemical Society Proceedings, Vol. 1999-19, 1999, pp. 513-521.

[24] Buchkremer, H., Diekmann, U., and Stöver, D, "Component Manufacturing and Stack Integration of Anode-supported Planar Sofc", System Proceedings of the Second European Solid Oxide Fuel Cell Forum, Vol. 1, 1996, pp. 221-228.

[25] V. M, J. O. Deutschmann, "Modeling of Solid-Oxide Fuel Cells", Z. Phys. Chem, Vol. 221, pp. 443–478.

[26] H. Tu, X. Liu and Q. Yu, "Synthesis and characterization of scandia ceria stabilized zirconia powders prepared by polymeric precursor method for integration into anode-supported solid oxide fuel cells", Journal of the Power Sources, vol. 196, 2011, pp. 3109-3113.

[27] M. Irshad, K. Siraj, R. Raza, A. Ali, P. Tiwari, B. Zhu, *et al.*, "A Brief Description of High Temperature Solid Oxide Fuel Cell's Operation, Materials, Design, Fabrication Technologies and Performance", Applied Sciences, vol. 6, 2016, p. 75.

[28]T. Franco, Z. Ilhan, M. Lang, G. Schiller, P. Szabo, "Investigation of Porous Metallic Substrates for Plasma Sprayed Thin-film Sofcs", The Electrochemical Society. Vol. 7, 2005, pp. 344-356.

[29] P. Holtappels, U. Stimming, Solid Oxide Fuel Cells (Sofc) in: Handbook of Fuel Cells, John Wiley & Sons, Ltd, New York, 2010, p. 453.

[30] Z.Tang, Y. Xie, H. Hawthorne, D. Ghosh, "Sol–gel Processing of Sr0.5 Sm0.5 CoO3 Film", Journal of Power Sources, Vol. 157, 2006, pp. 385-388.

[31] C. Xia, Y. Zhang, M. Liu, "Lsm-Gdc Composite Cathodes Derived from a Sol-gel Process Effect of Microstructure on Interfacial Polarization Resistance", Electrochemical and Solid-state Letters, Vol. 6, 2003, pp. A290-A292.

[32] H. Jinyan, ua. Kongfa, C. X. Huanga, N. A. Xiaobo, D. Chengwei, F. Jiaming, W. W. Sua,b,c, "Effect of composite pore-former on the fabrication and performance of anode-supported membranes for SOFCs", Journal of Membrane Science. Vol. 318, 2014, pp. 445–451.

[33] H. Shimada, E. Takami, K. Takizawa, A. Hagiwara, M. Ihara, "Highly dispersed anodes for solid oxide fuel cells using NiO/YSZ/BZY triple-phase composite powders prepared by spray pyrolysis", Solid State Ionics. Vol. 193, 2011, pp. 43–51.

[34] H. Liangfa, A. W. Chang, Y. Huang, "Porous Yttria-Stabilized Zirconia Ceramics with Ultra-Low Thermal Conductivity", Journal of Materials Science, Vol. 45, 2010, Pp. 3242–3246.

[35] W. Bao, Q. Chang, G, Meng. "Effect of NiO/YSZ compositions on the co-sintering process of anode-supported fuel cell", Journal of Membrane Science, Vol. 259, 2005, 103–109.

[36] D. Salehzadeh, M. Torabi, Z. Sadeghian, P. Marashi, "A multiscale-architecture solid oxide fuel cell fabricated by electrophoretic deposition technique" Journal of Alloys and Compounds, Vol. 830, 2020, pp. 1546-1554.

[37] J. W. Kim, A. V. Virkar, K. Z. Fung, K. Mehta, S. C. Singhal, (1999). Polarization effects in intermediate temperature, anode-supported solid oxide fuel cells. Journal of the Electrochemical Society. vol. 146, pp. 69-78.

[38] G. B. Jung, T. J. Huang, C.-L. Chang, "Effect of temperature and dopant concentration on the conductivity of samaria-doped ceria electrolyte", Journal of Solid State Electrochemistry, Vol. 6, 2002. pp. 225-230.

[39] S. Tao, J. T. Irvine, "A Redox-stable Efficient Anode for Solid-oxide Fuel Cells, *Nature Materials*. Vol. 2, 2003, pp. 320-323.

[40] T. L. Nguyen, T.Kato, Nozaki, T. Honda, A.Negishi, K. Kato, Y. Iimura, "Application of ($Sm_{0.5}Sr_{0.5}$) CoO_3 as a Cathode Material to (Zr, Sc) O_2 Electrolyte with Ceria-Based Interlayers for Reduced-temperature Operation Sofcs", Journal of the Electrochemical Society, Vol. 153, 2006. pp. A1310-A1316.

[41] Y. Zhang, "Fabrication and Characterisation of Planar and Tubular Solid Oxide Fuel Cell Anodes", Edinburgh Napier University", MSc by Research. Vol. 2, 2013, pp. 24-24.

[42] S. Singhal, "Advances in Solid Oxide Fuel Cell Technology", Solid State Ionics, Vol.135, 2000, pp. 305-313.

[43] H. Rob, W. Zhenwei, Olivera, W. Lars, R. Jasna, J. Sing, Y. Radenka, M. Dave, G. "Thermal plasma spraying for SOFCs: Applications, potential advantages, and challenges", Journal of Power Sources, Vol. 170, Issue 2, 2007, PP. 308-323**.**

[44] Y. Huang, J. Vohs, R. Gorte, "Sofc Cathodes Prepared by Infiltration with Various LSM Precursors. Electrochemical and Solid-State Letters", Vol. 9, 2006, pp. A237-A240.

[45] R. Gorte, H. Kim, J. M. Vohs, "Novel Sofc Anodes for the Direct Electrochemical Oxidation of Hydrocarbon" Journal of Power Sources",Vol. 106, 2002, pp. 10-15.

[46] M. Gross, M. D Vohs, R. J. Gorte, "A Study of Thermal Stability and Methane Tolerance of Cu-based Sofc Anodes with Electrodeposited Co", Electrochimical Acta. Vol. 52, 2007, pp. 1951-1957.

[47] H. A. Hamedani, M. Baniassadi, M.Khaleel, X. Sun, S. Ahzi, D. Ruch, H. Garmestani, "Microstructure, Property and Processing Relation in Gradient Porous Cathode of Solid Oxide Fuel Cells using Statistical Continuum Mechanics", Journal of Power Sources, Vol. 196, 2011, pp. 6325-6331.